Available online at www.sciencedirect.com
SCIENCE DIRECT®
International Journal of Heat and Fluid Flow 24 (2003) 444–453
International Journal of HEAT AND FLUID FLOW
www.elsevier.com/locate/ijhff

Symmetry breaking of flow and heat transfer in multiple impinging jets

L. Thielen *, H.J.J. Jonker, K. Hanjalić

Thermal and Fluids Sciences Section, Applied Physics, Delft University of Technology, Lorentzweg 1, 2628 CJ Delft, The Netherlands

Received 23 November 2002; accepted 8 February 2003

Abstract

This paper focuses on the effect of nozzle arrangement on the heat transfer of multiple impinging jets. Two different geometrical arrangements with an equal number of nozzles are studied, a square set-up (3×3 regularly spaced jets) and a circular set-up (eight jets surrounding a central jet). The predictions with two turbulence models are compared, the standard k–ε model with wall functions and Durbin's $\overline{v^2}$–f model [Theor. Comput. Fluid Dyn. 3 (1991) 1] with integration to the wall. Quite surprisingly we find for one of the arrangements—the square set-up—an asymmetric flow field, even though the geometry, as well as the initial and boundary conditions are perfectly symmetric. Both turbulence models predict this peculiar broken symmetry. The other arrangement—the circular set-up—behaves more in line of expectation: both turbulence models predict a flow field that reflects all the symmetries of the physical situation. Interestingly, the differences between the two arrangements are quite small, but the corresponding flow fields clearly exhibit marked differences. Although both turbulence models agree qualitatively quite well on the mean features of the flow field for the two different set-ups, there are significant quantitative differences between the models regarding the turbulent kinetic energy and heat transfer. In particular the peak values of both the kinetic energy and the Nusselt number are quite different. Finally, we make a detailed comparison between the resulting heat transfer of the different arrangements. In the circular set-up the individual jets have a similar heat transfer, except for the central jet which is stabilized by the outer jets. In the square set-up, the difference between the jets is much more pronounced: due to the aforementioned asymmetry, some jets impinge vigorously, with a high heat transfer at the expense of the other, deflected, jets.

Keywords: Multiple impinging jets; Turbulence modeling; Heat transfer; CFD

1. Introduction

Impinging fluid jets are used extensively by industry for efficient heating and cooling of solid surfaces. With a single jet a very high heat transfer can be achieved in the stagnation region, but further away from the stagnation point the heat transfer rapidly decreases. As a result the total heat transfer field is highly non-uniform. Therefore industrial applications usually make use of multiple impinging jets, which enhances the heat transfer over the desired area and improves its uniformity, while retaining the appealing properties of single jet heat transfer. The optimum performance of the single jet depends primarily on the jet-nozzle distance from the targeted wall and the intensity and structure of the turbulence in the jet. In multiple impinging jets, a new and important degree of freedom enters the optimization problem: the geometrical arrangement of the jets, viz. the distance between the jets (pitch), and the relative positioning (hexagonal arrangement, rectangular arrangement, etc.). If the spacing is too large, one ends up with many single jets, obviously with a poor heat flux uniformity. If they are too close, the jets start to influence each other (e.g. Geers et al., 2001), and may reduce the heat transfer significantly.

The objective of our study is twofold. First we study the effect of some geometrical arrangements of the jets on the flow field and thus on the heat transfer. Second we test the performance of different turbulence models. For a single impinging jet it has been shown that an accurate solution of the flow field is a necessary condition to obtain a good prediction of the resulting heat

* Corresponding author. Tel.: +31-15-2782470; fax: +31-15-2781204.
E-mail address: luuk@ws.tn.tudelft.nl (L. Thielen).

0142-727X/03/$ - see front matter © 2003 Elsevier Science Inc. All rights reserved.
doi:10.1016/S0142-727X(03)00042-0

transfer. For a single jet the quality of the prediction of different turbulence models has been found to vary drastically (e.g. Thielen et al., 2001). The flow field of a multiple impinging jet set-up is even harder to predict than the flow field of a single impinging jet, because of the 3-D effects, the anisotropy and the interaction between different jets. Therefore also for multiple impinging jets comparison of turbulence models is important. In this study we compare the predictions of two turbulence models, the standard k–ε model with wall functions and the $\overline{v^2}$–f model (Durbin, 1991) with integration to the wall. The $\overline{v^2}$–f model is based on the eddy-viscosity relationship; it uses $\overline{v^2}$ as an additional velocity scale, elliptic relaxation, which accounts for non-viscous wall blockage effects, and a switch of the scales from energy-containing to Kolmogorov, to account for viscosity effects very close to a wall. Therefore it solves two additional equations in comparison with the k–ε model, i.e. a transport equation for $\overline{v^2}$ and an elliptic equation for the elliptic relaxation parameter f. The model equations and the parameters can be found in Appendix A.

2. Case description

Two geometrical arrangements of nozzles have been studied (Fig. 1), referred to as "square" set-up (1(a)) and "circular" set-up (1(b)). Both the square set-up and circular set-up consist of nine nozzles and possess the same axes of symmetry, i.e. along 0°, 45° and 90°. Because of symmetry, calculations can be done on one quarter of the full geometry, as indicated by the shaded area in Fig. 1. Actually, the calculations could have been carried out even on 1/8th of the full geometry, but, for convenience of grid generation, we did not exploit this additional symmetry along the 45° axis. This redundant symmetry therefore remains in the computational domain, with the obvious expectation that the predicted flow field will reflect this symmetry. The dimensions of both set-ups are the same: the distance from the nozzle plate to the impingement plate is $4D$, with D the nozzle diameter, i.e. $H = 4D$. The spacing between the nozzles for the square set-up and the spacing between the central jet and the surrounding jets for the circular set-up is $4D$. This leads to the domain and boundary conditions as shown in Fig. 1(c). The top is the plane with the nozzles, the bottom is the impingement plane. Two sides have symmetry boundary conditions, the outlets have a prescribed pressure boundary condition. The Reynolds-number, based on the bulk velocity and the nozzle diameter is 20.000. At the inlet uniform profiles for all the variables are assumed. The edges of the domain are at $8D$ from the center of the domain.

The in-house CFD code used, called X-Stream, is designed for the RANS equations and these equations are solved using a multi-block, structured finite volume method and the code is parallelized using MPI. The pressure–velocity coupling is solved with the SIMPLE algorithm (Patankar, 1980). The ILU solver (Stone, 1968) has been used for solving the system of linear equations. The convective terms in the equations are approximated using a blending scheme between upwind and central differencing. For the k–ε calculations the grid consisted in total of around 80.000 cells. This resulted in an average y^+ value of 40 for the first computational node above the impingement wall. A uniform grid was used in the wall-normal direction. To test the grid dependence, also computations were performed on a finer grid, in which every cell was subdivided in eight cells. The results did not differ significantly, so the first grid was chosen for the computations. In the $\overline{v^2}$–f model equations are integrated to the wall and therefore a finer mesh near the wall is required. Therefore the grid used consists of approximately 300.000 volumes and the average y^+ value for the first computational node above the impingement wall is 5. The grid was clustered near the impingement wall. For this case both a coarser and a

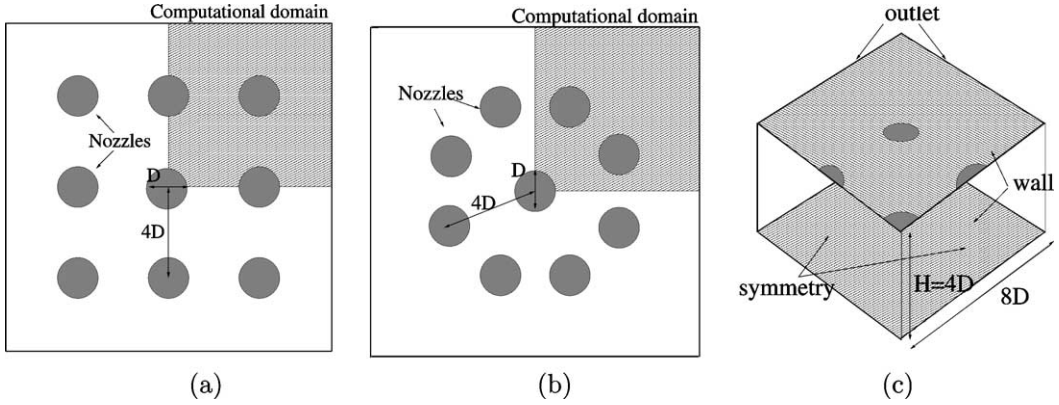

Fig. 1. Top view of the two geometrical arrangements of nozzles, (a) square set-up, (b) circular set-up, and (c) the domain and the boundary conditions.

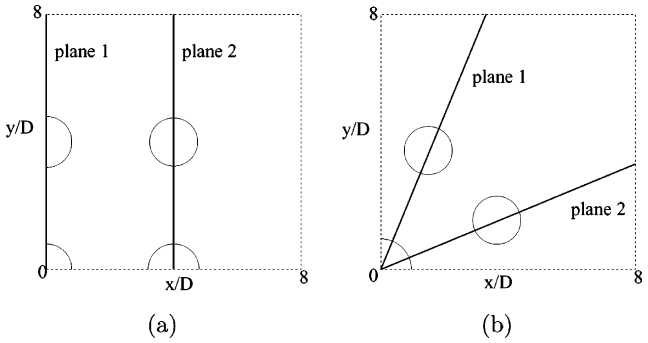

Fig. 2. Position of the visualization planes, (a) square set-up, (b) circular set-up.

finer grid were also tested. The intermediate grid was found to be sufficiently fine enough. The results are visualized on planes in the domain. The position of these planes for the square and circular set-up are depicted in Fig. 2.

3. Results

3.1. Square set-up

The pathlines are shown in Fig. 3 for the calculations with the k–ε model. The jets can be seen to leave the nozzle exits and flow down towards the impingement plate. In the stagnation region the jets are decelerated and deflected. A wall jet, parallel to the impingement plate, is formed. At the points where the wall jets meet, an up-wash is created. Here the flow is going up towards the nozzle plate, where it is again deflected and flows along the top plate to the edge of the domain.

Both in Fig. 3(a) and (b) one clearly observes that the computed flow field is not symmetric along the 45° axis. Apparently, and contrary to what was hinted at in the previous section, the predicted flow pattern *does not* reflect the additional symmetry still residing in the geometry and boundary conditions. Instead, a vortex develops (only) near the upper left nozzle, see Fig. 3(b). As a result the jet from this nozzle is deflected outwards (Fig. 3(a)). This deflection can be clearly seen in Fig. 4, which shows the velocity component normal to the impingement wall (positive upward) in plane 1 (see Fig. 2).

Both the k–ε and $\overline{v^2}$–f model predict a deflection outwards. As a result, the outer jet does not impinge straight below the nozzle exit. Also the up-wash region between the jets can be observed. The turbulent kinetic energy in plane 1 is plotted in Fig. 5. The results reveal the shear layer at the edges of the jet. The disturbed jet can be clearly seen in the position of the shear layers of the outer jet. To show that the disturbance is only present near the upper left nozzle, in Fig. 6 the turbulent kinetic energy in plane 2 is plotted. Both jets are undisturbed and impinge normally on the plate.

The observed asymmetric solution of the flow field is very surprising and puzzling in our view. But unfortunately the origin of the phenomenon is (at present) not clear to the authors. We note that both turbulence models, at least in a qualitative sense, agree on the mean features of the flow. Of course, the first obvious explanation would be a bug in the numerical code. Therefore special care has been taken to be certain the asymmetry is not a (simple) numerical artefact. Firstly, since the results presented thus far involved steady calculations, we considered unsteady calculations. Then also a vortex would develop, which wiggled around a bit, until it would eventually settle into a steady state similar to the

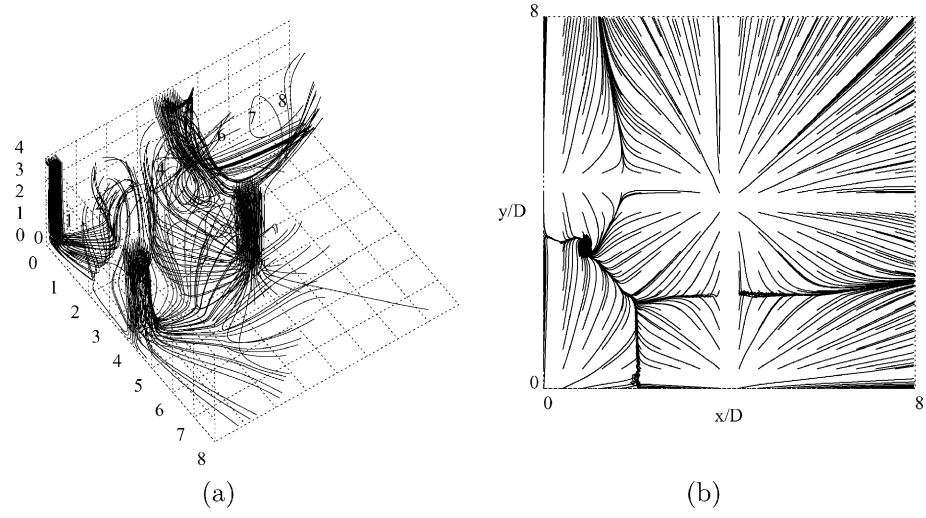

Fig. 3. Pathlines for the square set-up, as predicted by the k–ε model, (a) in the computational domain and (b) at $0.01D$ above the impingement plane. One can clearly observe the asymmetry in the predicted flow field. A vortex has developed near the top-left jet (see (b)); this jet is disturbed and deflected outwards (a).

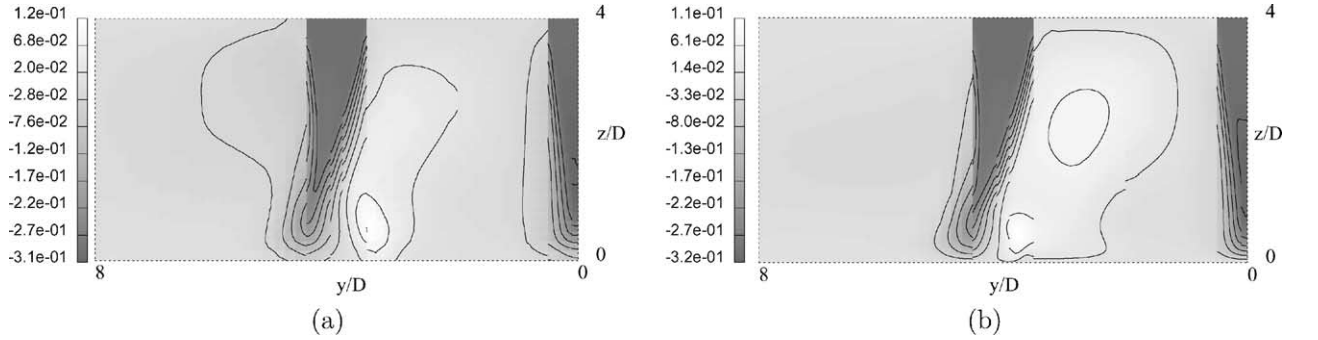

Fig. 4. Wall-normal velocity component in plane 1, for the square set-up; predictions by two turbulence models, (a) k–ε, (b) $\overline{v^2}$–f. The outer jet is deflected.

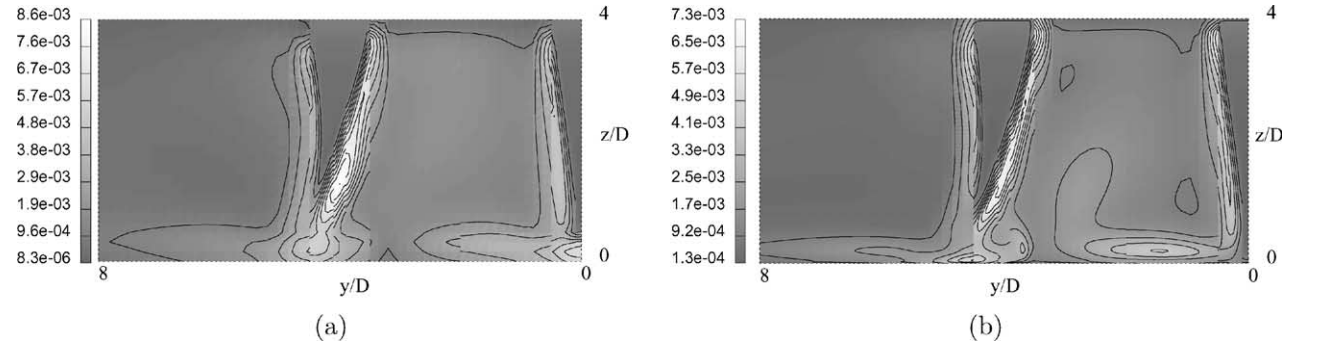

Fig. 5. Turbulent kinetic energy in plane 1, for the square set-up; predictions by two turbulence models, (a) k–ε, (b) $\overline{v^2}$–f. The shear layers show the disturbed jet. The position of regions with high turbulent kinetic energy differs between the two models.

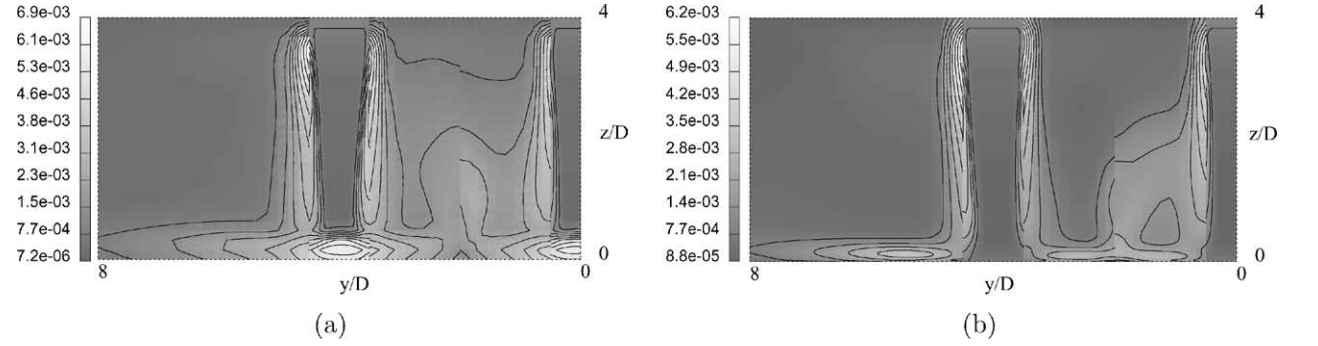

Fig. 6. Turbulent kinetic energy in plane 2, square set-up; predictions by two turbulence models, (a) k–ε, (b) $\overline{v^2}$–f. One can clearly observe the differences between the two turbulence models: higher peak values with the k–ε model and different locations of regions with high turbulent kinetic energy.

reported steady calculations. Secondly, since for the convective terms blending between upwind and central differencing was applied, we varied the blending factors. The calculations would be started with typically 10% of central differencing for all variables. The results then already exhibit the broken symmetry. All final results are obtained with 80% of central differencing for the flow variables and 70% for the turbulent quantities. Variation of these values only entailed marginal changes. Thirdly, we looked at grid dependence. For the calculations with the $\overline{v^2}$–f model both a coarser and a finer grid were tested. The average y^+ value for the first computational node above the impingement wall was around 12 for the coarse grid and around 3 for the fine grid. Still the calculations on these grids would converge to an asymmetric solution very similar to the intermediate grid calculations. Next, because the vortex tended to emerge always at the same location (near the upper left jet in Fig. 2(a)), which is odd since there should not be any preference due to symmetry in the physical situation, we did a number of checks: (a) we started with a symmetric initial field constructed by mirroring the

solution from one half of the domain from the previous computation: the asymmetry would soon develop again; (b) we started with two vortices, again constructed from the previous results: one vortex would disappear; (c) we mirrored the solution along the 45° axis: nothing would change. Other calculations also revealed that the vortex has equal chance to develop on either side of the 45° line. All in all, we concluded there is no specific preference of the vortex on which side of the diagonal it appears. Another check was the computation of the full domain for the square set-up (i.e. the entire domain depicted in Fig. 1(a)). For this set-up no symmetry boundary condition is used. As shown in Fig. 7(b) also the flow field in the full set-up exhibits a broken symmetry. Due to the interaction of the jets, some jets are disturbed. This is more clear from Fig. 8, which shows the wall-normal velocity component in two planes (see Fig. 7(a)). The left jet in plane 2 is pushed outwards, while the jets in plane 1 are undisturbed.

Finally, we checked our results with a different code. To this end we repeated the calculations with the k–ε model using the commercial CFD code FLUENT. These calculations (Aubel et al., 2001) exhibited the same asymmetry and were in excellent agreement with the k–ε results presented above. At this point we therefore conclude that the asymmetry is not a numerical artefact. We come back to this issue in the discussion.

So far we have stressed similarities between the results of the two turbulence models, however, close inspection yields a number of significant differences. For a single impinging jet the k–ε model is known to largely overpredict the turbulent kinetic energy in the stagnation region and as a result also the heat transfer is overpredicted (e.g. Thielen et al., 2001). The multiple impinging jet results seem to exhibit the same deficit, as can be seen in the stagnation region of both the center and the outer jet in Fig. 6. The k–ε model gives peak values in these regions. The $\overline{v^2}$–f model does not show this deficiency and predicts the maximum of k in the shear layer and the wall jet. Also the peak value with the k–ε model is higher than with the $\overline{v^2}$–f model.

3.2. Circular set-up

In Fig. 9 the pathlines for the circular set-up are presented. Note that the circular set-up has the same number of nozzles and possesses the same axes of symmetry as the square set-up (see Fig. 1). However, the calculations for this set-up do not exhibit any anomaly and appear to nicely reflect the symmetry along the 45° axis, as one would expect. The two outer jets are slightly curved in the middle of the domain, but still impinge straight below the nozzle exit. This can be seen better in Fig. 10, where the wall-normal velocity component (positive upward) in planes 1 and 2 is shown.

The up-wash in between the jets can be observed. The outer jets are pushed outwards in the middle. It also shows the symmetry in the solution: The two planes 1 and 2 give similar solutions. Therefore in the sequel only the solution in plane 2 will be shown.

The turbulent kinetic energy in plane 2 is plotted in Fig. 11. Again the shear layers at the edge of the jet can be clearly seen. These results again reveal the differences between the models, i.e. different peak values and

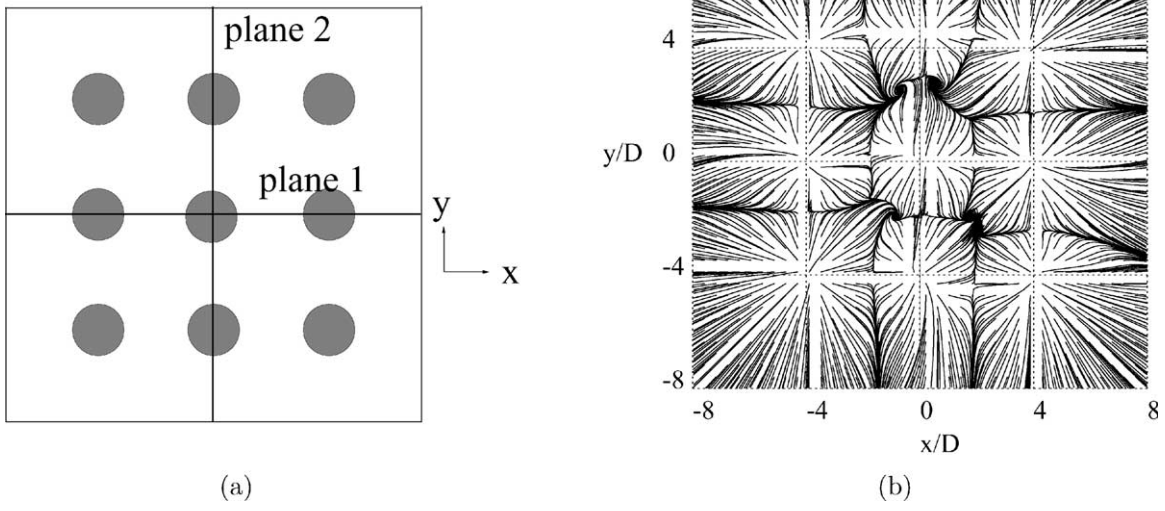

Fig. 7. In (a) the position of the visualization planes for the full square set-up is shown. In (b) the pathlines in a plane at $0.01D$ above the impingement plane, as predicted by the k–ε model, are visualized. The pathline pattern looks similar to what one would expect from mirroring the solution of Fig. 3(b).

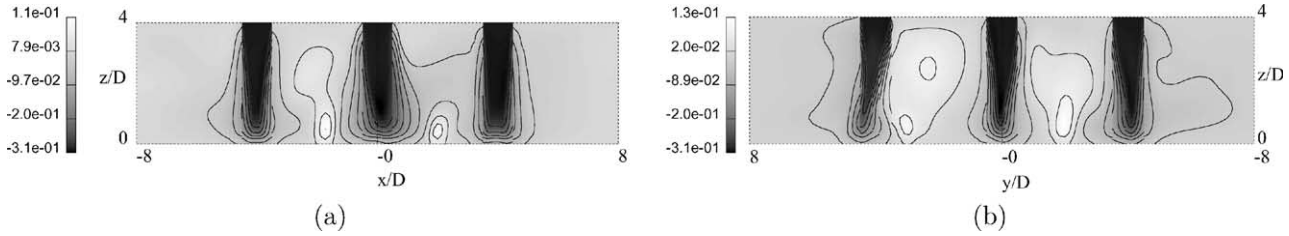

Fig. 8. Wall-normal velocity component in planes 1 (a) and 2 (b) for the full square set-up, as predicted by the k–ε model. The left jet in plane 2 clearly is disturbed.

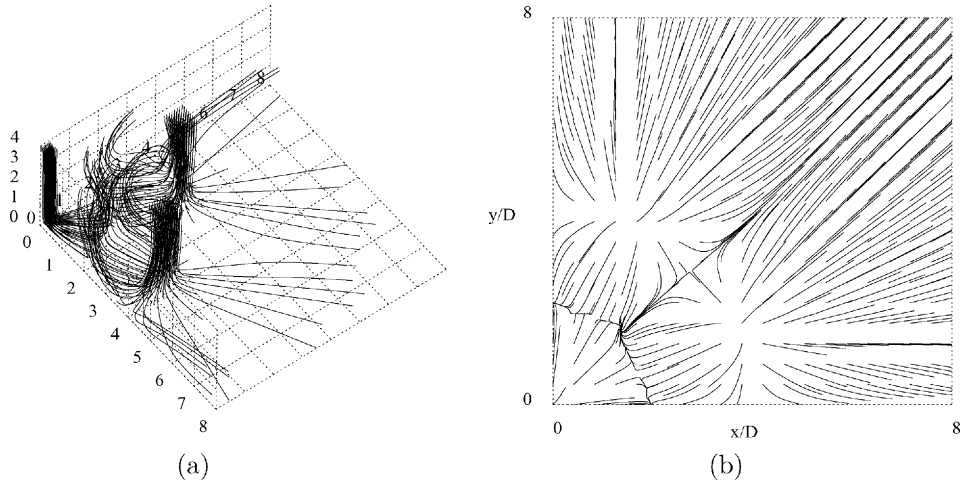

Fig. 9. Pathlines for the circular set-up, as predicted by the k–ε model, (a) in the computational domain and (b) at $0.01D$ above the impingement plane. The symmetry in the flow field can be observed.

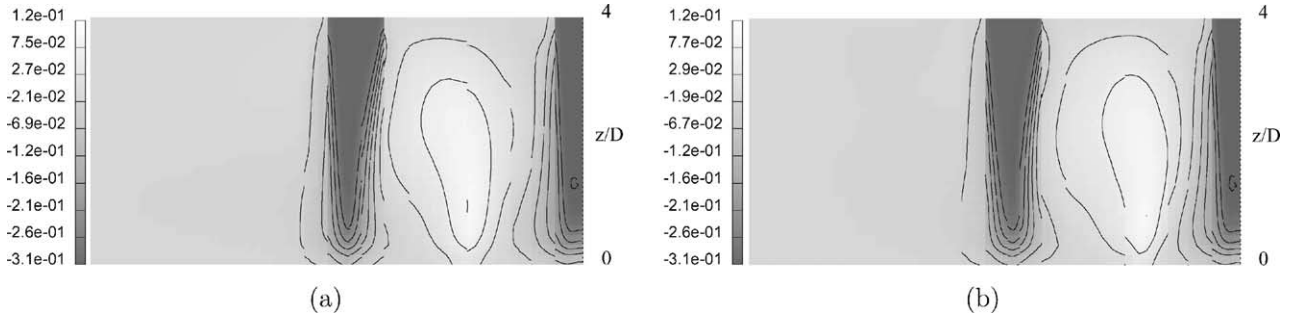

Fig. 10. Wall-normal velocity component, result of the k–ε model for circular set-up. (a) Plane 1, (b) plane 2. The results of the two different planes again reveal the symmetry in the flow field.

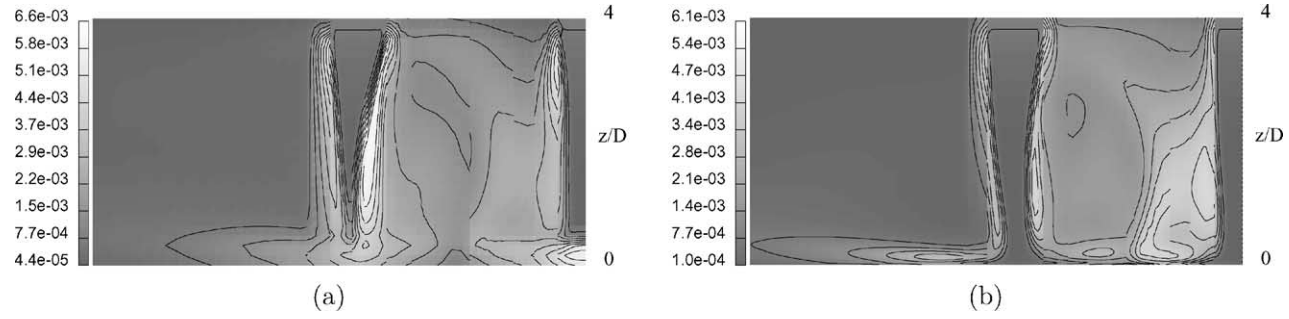

Fig. 11. Turbulent kinetic energy in plane 2, circular set-up; predictions by two turbulence models, (a) k–ε, (b) $\overline{v^2}$–f. The predictions between the turbulence models are clearly different: different peak values are predicted and the locations of regions with high turbulent kinetic energy are different.

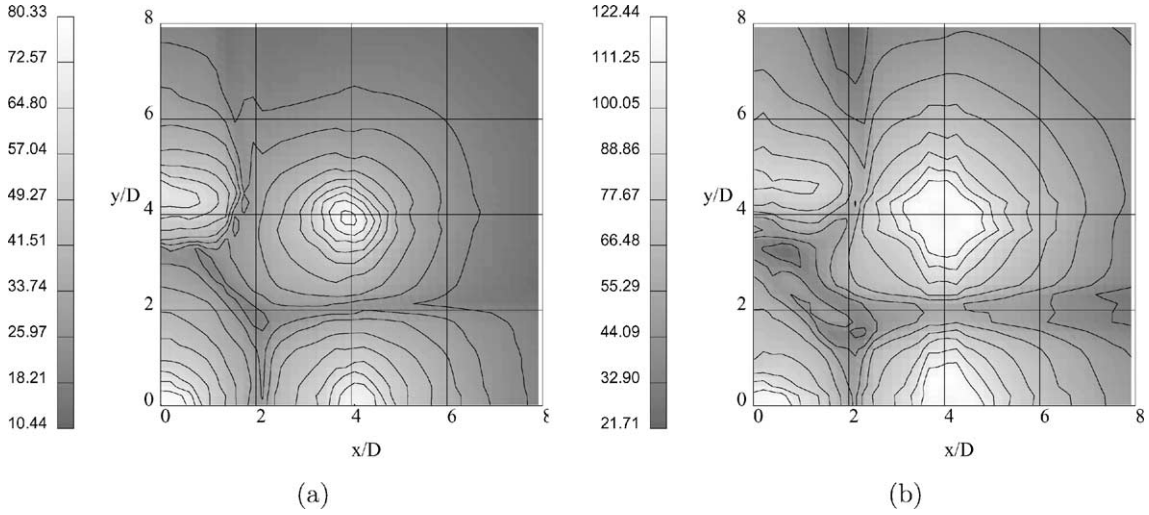

Fig. 12. Nusselt number distribution, square set-up; predictions by two turbulence models, (a) k–ε, (b) $\overline{v^2}$–f. Note the difference in contour values between (a) and (b). The disturbed jet loses some of its heating/cooling capacity. The k–ε model predicts a small peak in the stagnation point (a). The $\overline{v^2}$–f model results shows a larger region with a high Nusselt number (b).

different locations of regions with high turbulent kinetic energy. For the k–ε model these regions are the shear layer of the jets and the stagnation regions, while the $\overline{v^2}$–f model predicts these regions in the shear layer and the wall jet.

3.3. Heat transfer

For both set-ups the resulting heat transfer on the impingement plane was calculated, using both turbulence models. For the turbulent heat flux the isotropic eddy diffusivity formulation was used:

$$\overline{\theta u_i} = -\frac{\nu_t}{\sigma_t}\frac{\partial \Theta}{\partial x_i} \tag{1}$$

with σ_t the turbulent Prandtl number $= 0.9$. In Fig. 12 the Nusselt number distribution on the impingement plane for the square set-up is plotted. The disturbed jet loses some of its heating/cooling capacity. Both models predict the peak value of the Nusselt number to be about 20% less than that of the undisturbed jets. Because the k–ε model predicts peak values for the turbulent kinetic energy in the stagnation region, also a peak value for the Nusselt number can be seen. The $\overline{v^2}$–f predicts high turbulent kinetic energy in the wall jet. As a result the peak values of the Nusselt number appear in a larger area of the stagnation region.

For the circular set-up the Nusselt number distribution can be seen in Fig. 13. It again reveals the symmetry in the results. Note however that the peak value of the

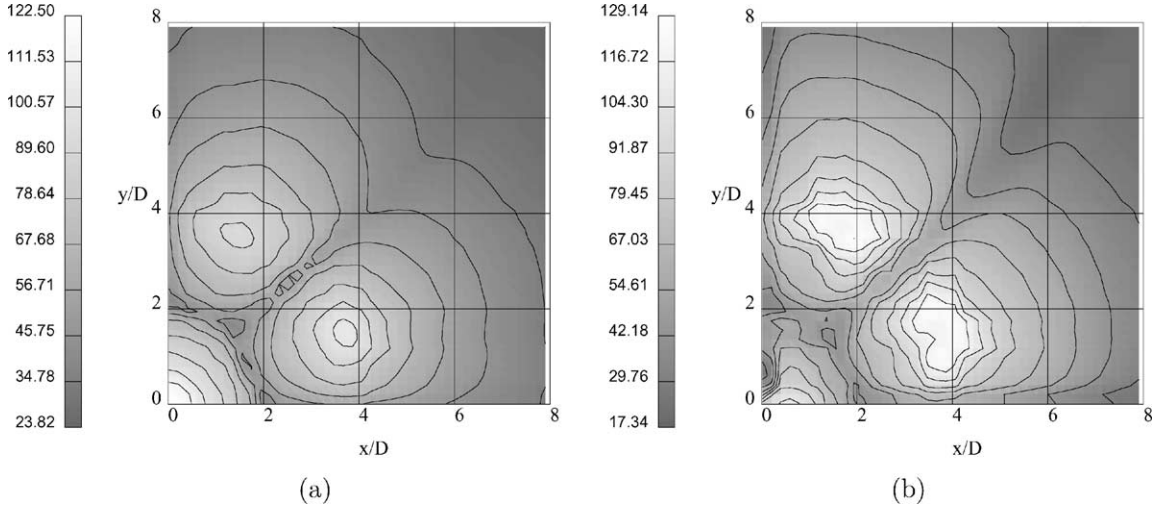

Fig. 13. Nusselt number distribution, circular set-up; predictions by two turbulence models, (a) k–ε, (b) $\overline{v^2}$–f. Both models predict a higher peak value for the central jet, which seems to be stabilized and enforced by the outer jets.

outer two jets is predicted to be lower than the peak value of the central jet. The outer jets seems to stabilize and enforce the central jet. The $\overline{v^2}$–f model results again show the peaks in Nusselt number in a larger area of the stagnation region.

4. Conclusions

In this paper the effect of geometrical arrangement of nozzles in a multiple impinging jet set-up on the flow field and resulting heat transfer was studied. The results of two turbulence models (the k–ε model and $\overline{v^2}$–f model) have been compared. We studied a square set-up and a circular set-up, both consisting of nine nozzles. Quite surprisingly the square set-up results revealed an asymmetric flow field in a situation where the geometry and boundary conditions were symmetric. A vortex develops near (only) one of the nozzles and as a result this jet is deflected. Consequently also the heat transfer of this jet is deteriorated. In contrast, the results for the circular set-up, which has the same number of jets and has the same axes of symmetry, appeared to be symmetric.

The occurrence of the asymmetric solution is puzzling and raises some questions on the general applicability of symmetry boundary conditions, as elaborated below. In our study we made use of two out of three symmetries present in the physical situation. We therefore applied only two symmetry boundary conditions but did not exploit the third symmetry (for convenience of grid generation). But suppose we *had* made use of the third symmetry. The resulting flow field would then have been symmetric *by construction*. This implies that we would have missed a very prominent feature of the flow field. The central question then becomes: How can one decide whether this is the case or not just by looking at the computations? By the same line of reasoning we must ask ourselves in retrospect whether the application of the other two symmetries were justified or not. Computations of the full geometry are not entirely conclusive. At first sight, they seem to justify the application of the two symmetry boundary conditions, because the pathline pattern (Fig. 7(b)) looks similar to what one would expect from mirroring the solution of Fig. 3(b). However, the lower right quarter (still) deviates from this expectation. It is also puzzling why the circular set-up does not yield any anomalies. The differences between the set-ups are only minor; in fact, the circular set-up can be obtained from the square set-up just by moving the diagonal nozzle jet slightly to the middle. If one does this gradually, one must find a transition point in between where the asymmetry vanishes. Simulations of this effect indicate that already a marginal displacement of the diagonal nozzle to the center results in a symmetric flow field. This remains the case for all intermediate set-ups, up to the circular set-up. Interestingly, however, first results of PIV measurements of the flow field in the square set-up also reveal an asymmetric occurrence of a vortex, see Fig. 14 (L. Geers, personal communication).

Corroborating the notion that the asymmetry is physical, another question is how it is possible in numerical simulations to have a symmetric initial field and symmetric boundary conditions and yet to end up with an asymmetric solution? Minor disturbances can arise in

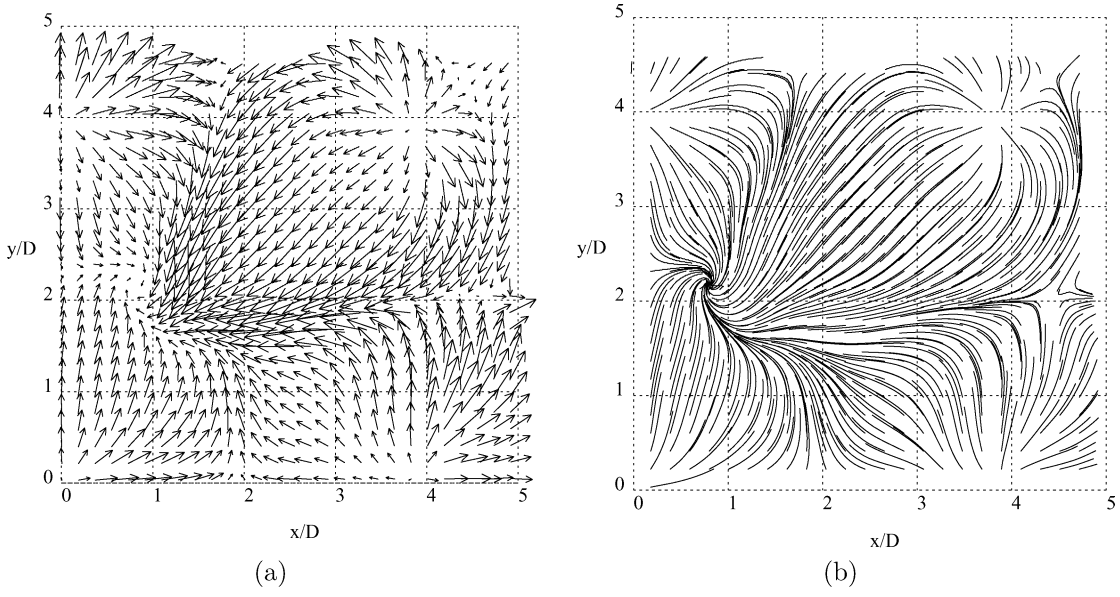

Fig. 14. Average velocity field of the square set-up at 0.54D above the impingement plane, obtained from PIV measurements (*courtesy L. Geers*); (a) velocity vectors, (b) pathlines. These can be compared with the results of the computations in Fig. 3(b). The broken symmetry can be observed. A vortex is present near the upper left nozzle.

the simulations because the system of linearized equations is solved in an iterative and non-symmetric manner. Apparently, in the square set-up, this small asymmetry can then develop further. But in the circular set-up, solved with the same procedure, apparently the physics of the flow field suppresses these numerical disturbances. So although the asymmetry originates from the numerics, the asymmetry present in the final solution is nevertheless a physical phenomenom. With that in mind, it is worth considering to start a computation of a symmetrical domain and with symmetric boundary conditions with *an asymmetric* initial field (for instance by adding a small amount of noise). If the final solution is then symmetric it is surely a realistic solution representing the physics. Moreover, if an asymmetric solution develops, this is also caused by the physics and not by the numerical procedure, since the numerical errors are much smaller than the noise.

Two turbulence models have been used in this study, the k–ε model and the $\overline{v^2}$–f model (Durbin, 1991). Qualitatively the overall prediction of the flow field is comparable for both models. For the turbulent kinetic energy there are differences. The k–ε model predicts higher peak values than the $\overline{v^2}$–f model. As a result the predicted heat transfer is higher with the k–ε. Also the position of regions with high turbulent kinetic energy is different. The k–ε model shows high values in the shear layer of the jet and the stagnation region. The $\overline{v^2}$–f model predicts high values in the shear layer and the wall jet. The observed differences between the two models are similar to what was found for a single impinging jet (Thielen et al., 2001).

Regarding heat transfer, an important question is which of the two geometries has the best heat transfer characteristics. In the square set-up, the remaining undisturbed jets have the same peak value of the Nusselt number as the central jet. In the circular set-up the outer jets have a lower value than the central one. So it seems that, by disturbing one jet, the other jets keep their full heating/cooling potential. The peak value of the Nusselt number of the central jet in the circular set-up is higher than the peak value of the central jet in the square set-up. The different predictions for the turbulent kinetic energy by the two turbulence models, results in different shapes for the heat transfer distributions. The k–ε model gives a peak value at the stagnation point, where also the kinetic energy has a maximum. The $\overline{v^2}$–f model, which predicts high kinetic energy values in the wall jet, predicts a larger region of high heat transfer in the stagnation region.

Acknowledgements

This work was sponsored by the Technology Foundation (STW) and the National Computing Facilities Foundation (NCF) for the use of supercomputer facilities, with financial support of NWO.

Appendix A

In the $\overline{v^2}$–f model transport equations are solved for k, ε, $\overline{v^2}$ and f. These equations are given by:

$$\frac{\mathrm{D}k}{\mathrm{D}t} = \frac{\partial}{\partial x_i}\left[\left(\nu + \frac{\nu_\mathrm{t}}{\sigma_\mathrm{k}}\right)\frac{\partial k}{\partial x_i}\right] + P_\mathrm{k} - \varepsilon$$

$$\frac{\mathrm{D}\varepsilon}{\mathrm{D}t} = \frac{\partial}{\partial x_i}\left[\left(\nu + \frac{\nu_\mathrm{t}}{\sigma_\varepsilon}\right)\frac{\partial \varepsilon}{\partial x_i}\right] + \frac{C'_{\varepsilon 1}P_\mathrm{k} - C_{\varepsilon 2}\varepsilon}{T}$$

$$\frac{\mathrm{D}\overline{v^2}}{\mathrm{D}t} = \frac{\partial}{\partial x_i}\left[\left(\nu + \frac{\nu_\mathrm{t}}{\sigma_\mathrm{k}}\right)\frac{\partial \overline{v^2}}{\partial x_i}\right] + kf - \frac{\overline{v^2}}{k}\varepsilon$$

$$f = L^2\frac{\partial^2 f}{\partial x_i^2} + (C_1 - 1)\frac{\left(\frac{2}{3} - \frac{\overline{v^2}}{k}\right)}{T} + C_2\frac{P_\mathrm{k}}{k}$$

where P_k is the production of turbulent kinetic energy and is given by

$$P_\mathrm{k} = 2\nu_\mathrm{t}\left(\frac{\partial U_i}{\partial x_j} + \frac{\partial U_j}{\partial x_i}\right)^2$$

The expression for the eddy-viscosity is $\nu_\mathrm{t} = C_\mu\overline{v^2}T$. In these equations T is a time scale and L is a length scale, which are calculated by the standard formulations and the realizability constraints (Durbin, 1996):

$$T = \min\left(T'; \frac{\alpha}{\sqrt{6}}\frac{\overline{v^2}k}{C_\mu\sqrt{S_{ij}^2}}\right) \quad T' = \max\left(\frac{k}{\varepsilon}; 6\left(\frac{\nu}{\varepsilon}\right)^{1/2}\right)$$

$$L = \min\left(L'; \frac{1}{\sqrt{6}}\frac{\overline{v^2}k^{3/2}}{C_\mu\sqrt{S_{ij}^2}}\right) \quad L' = C_L\max\left(\frac{k^{\frac{3}{2}}}{\varepsilon}; C_\eta\left(\frac{\nu^3}{\varepsilon}\right)^{1/4}\right)$$

Here α is a model parameter and comparison with experimental data for a single impinging jet indicates that $\alpha = 0.6$ is the optimum value (Behnia et al., 1996). The other parameters of the model are:

$$C'_{\varepsilon 1} = 1.4\left(1 + 0.045\left(\frac{k}{\overline{v^2}}\right)^{1/2}\right)$$

C_μ	$C_{\varepsilon 2}$	C_1	C_2	C_L	C_η	σ_k	σ_ε
0.22	1.9	1.4	0.3	0.25	85.0	1.0	1.3

The boundary conditions at a solid wall are:

$$k = 0; \quad \overline{v^2} = 0; \quad \varepsilon = \frac{2\nu k_\mathrm{p}}{y_\mathrm{p}^2}; \quad f = -\frac{20\nu^2\overline{v^2}_\mathrm{p}}{\varepsilon y_\mathrm{p}^4}$$

where the subscript p means first computational point near the wall.

References

Aubel, T., Thielen, L., Jonker, H.J.J., 2001. Numerical study of the flow in multiple impinging jets. Technical Report APTF-R/01-06, Technical University Delft.

Behnia, M., Parneix, S., Durbin, P., 1996. Simulation of jet impingement heat transfer with the k–ϵ–v^2 model. Annual research brief of the Center for Turbulence. pp. 3–16.

Durbin, P.A., 1991. Near-wall turbulence closure modeling without damping functions. Theor. Comput. Fluid Dyn. 3, 1–13.

Durbin, P.A., 1996. On the k–ϵ stagnation point anomaly. Int. J. Heat Fluid Flow 17 (1), 89–90.

Geers, L.F.G., Tummers, M.J., Hanjalić, K., 2001. PIV measurements in impinging jets at a high Reynolds number. In: Proceedings of the Second International Symposium on Turbulence and Shear Flow Phenomena, vol. II. pp. 289–294.

Patankar, S.V., 1980. Numerical Heat Transfer and Fluid Flow. Hemisphere Publishing Corporation.

Stone, H.L., 1968. Iterative solution of implicit approximations of multi-dimensional partial differential equations. SIAM J. Numer. Anal. 5, 530–558.

Thielen, L., Jonker, H., Manceau, R., Hanjalić, K., 2001. Turbulence modelling in a single normally impinging jet. In: Proceedings of the Fourth International Symposium on Computational Technologies for Fluid/Thermal/Chemical Systems with Industrial Applications, Atlanta 2001, vol. 424-1. pp. 239–246.